# Test of the Upgraded IRAC1 Camera for 1–5 $\mu$m Imaging

*A. MOORWOOD, G. FINGER, ESO-Garching, and H. GEMPERLEIN, ESO-La Silla*

## 1. Status

IRAC1 has been upgraded with an SBRC 58 × 62 pixel InSb array sensitive from 1 to 5.4 $\mu$m and was reinstalled and tested at the F/35 infrared focus of the 2.2-m telescope in May 1994. It is now being offered primarily (i) to complement IRAC2 (1–2.5 $\mu$m) at the 2.2-m and TIMMI (8–17 $\mu$m) at the 3.6-m by providing for L(3.8 $\mu$m) and M(4.7 $\mu$m) band and 3–4.5 $\mu$m CVF (Circular Variable Filter) narrow-band ($R \sim 50$) imaging and (ii) to replace the decommissioned infrared photometers for 1–2.5 $\mu$m photometry of objects too bright for IRAC2 ($K \leq 6$). It also provides the capability for obtaining photometry of objects over the complete 1–5 $\mu$m range without switching cameras. Using solid-nitrogen cooling for which this camera was originally designed, however, its performance is background limited in the thermal infrared but detector dark current limited at the shorter wavelengths with the new array. Although we have confirmed that this problem can be overcome with liquid-helium cooling, we have not managed to achieve a holding time sufficient to avoid refilling during the night thus increasing the operational overhead on La Silla. As IRAC2 is still expected to remain the instrument of choice for most 1–2.5 $\mu$m imaging applications due to its larger array (256 × 256) and superior sensitivity over this range, it is currently foreseen that nitrogen cooling will be considered the norm unless there are scientifically justifiable reasons for enhanced short-wavelength performance with IRAC1.

## 2. Observing Modes

IRAC1 provides for imaging through broad-band, narrow-band and Circular Variable (CVF) filters between 1 and 5 $\mu$m at two selectable pixel scales as summarized in Table 1.

Observations can be made in DC (staring) mode or with secondary-mirror sky chopping, and both modes can be combined with telescope nodding. Tests at the telescope (see below) confirmed that optimum performance in the broad/narrow-band filters at > 3 $\mu$m requires sky chopping while observations in the shorter wavelength filters and the CVFs are generally best made in the *dither* mode. In the latter case, a sequence of images recorded at different telescope positions is used to construct both the final object and sky frames. Such sequences can now be executed automatically using the IRAC sequencer and the combined telescope/guide probe offset feature introduced in May which maintains the TV autoguiding without manual intervention.

TABLE 1. *IRAC1 Camera Characteristics*

| Image Scales and Fields | | |
|---|---|---|
| Objective | arcsec/pix | arcsec |
| L4 | 0.45 | 26×28 |
| S3 | 0.8 | 46×49 |
| **Filters** | | |
| Name | $\lambda(\mu m)$ | $\Delta\lambda(\mu m)$ |
| J | 1.25 | 0.3 |
| H | 1.65 | 0.3 |
| K | 2.2 | 0.4 |
| PAH | 3.3 | 0.16 |
| PAH ref. | 3.3 | 0.8 |
| L′ | 3.75 | 0.7 |
| LN1 | 3.7 | 0.1 |
| LN2 | 3.83 | 0.2 |
| MN1 | 4.7 | 0.1 |
| MN2 | 4.7 | 0.17 |
| CVF 1 | 1.5–2.5 $\mu$m | $\lambda/\Delta\lambda \sim 50$ |
| CVF 2 | 2.5–4.5 $\mu$m | $\lambda/\Delta\lambda \sim 50$ |

## 3. Test Results

### 3.1 Emissivity

Telescope emission is expected to dominate the background and hence set the performance limits in the thermal infrared. Measurements of the total background at the 2.2-m with the photometer have implied a relatively high emissivity of ~ 0.2 compared e.g with ~ 0.13 at the 3.6-m and have led to some speculation regarding a possible additional, unidentified source of thermal background emission. In order to investigate this further, we included a series of measurements designed to separate the various background contributions. These included measurements with the camera viewing (i) a liquid-nitrogen-cooled blackbody, (ii) the sky directly with the camera located outside the telescope dome, (iii) the telescope + sky, and (iv) a black plate at ambient temperature. The results indicate that the camera entrance window contributes a few per cent and yielded the sky and telescope emissivities summarized in Table 2.

TABLE 2. *Sky and Telescope Emissivities*

| Filter | Sky | Telescope |
|---|---|---|
| L′ (3.75 $\mu$m) | 0.03 | 0.15 |
| LN1 (3.7 $\mu$m) | 0.007 | 0.16 |
| MN1 (4.7 $\mu$m) | 0.09 | 0.13 |

In assessing the telescope emissivity values it should be noted that the absolute minimum that could be expected is ~ 0.08 from the telescope mirrors, spider and adapter dichroic assuming the mirrors are clean. In addition, however, the 2.2-m telescope has a large central primary hole which could contribute up to ~ 0.08 additionally and which we have attempted to minimize by mounting a mirror, which views the cold camera, at the centre of the secondary. Given the uncertainties in estimating the individual sources of telescope emissivity, however, it appears that the measured values are consistent with assuming more realistic operational values for the mirrors and incomplete rejection of thermal radiation from the central obstruction without invoking additional unidentified sources. At the longest wavelengths, in the M band, the sky contribution becomes comparable to that of the telescope even in the narrow-band filter centred in the best part of the atmospheric window.

### 3.2 Sky chopping

The question as to whether or not sky chopping with array detectors is necessary in the thermal infrared and, if so, at what frequency, has become a much debated issue and one of particular importance for the design of the next-generation large telescopes where chopping the secondary mirrors presents a considerable technical challenge. Both to optimize the performance of IRAC1 at the 2.2-m and with an eye also to the VLT, we have investigated this aspect by measuring noise as a function of frequency in the L′(3.75 $\mu$m) band. The results are shown plotted in Figure 1 where the "high" frequency points were obtained with secondary-mirror chopping and the low-frequency ones by nodding the telescope and the total measurement time is the same at each frequency.

The result clearly shows a rapid decrease in noise with increasing chopping frequency up to ~ 2 Hz where it flattens

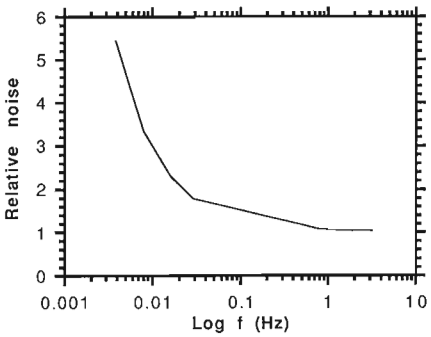


Figure 1: *Relative noise versus chopping frequency using the L′ (3.75 μm) filter and the same total measurement time.*

off at the value to which this curve is normalized and which was found to correspond to the expected shot noise on the measured background. At this background level (which is very similar to that in MN1 also) the detector half full well capacity is reached in ∼0.075 s so there is no conflict with the chopping requirement. At the much lower backgrounds experienced at wavelengths < 3 μm and when using the CVFs, however, it is necessary to utilize longer detector integration times (up to DIT ∼60 s) together with telescope nodding or "dithering" every ∼1 minute, rather than chopping to reach the backround limits.

### 3.3 Detection limits

Due to poor weather during the telescope tests, the performance could not be measured in all modes and the magnitude limits given below are therefore a mixture of directly measured and derived values as specified.

Table 3 summarizes the 3σ detection limits in the 3–5 μm range expressed as mag/sq. arcsec obtained in 2 × 60 s total measurement time. They are background limited and the values given were measured with a relatively high telescope temperature ∼13 C. These are also worst-case values in the sense that the chopping amplitude was larger than the field, i.e the object integration time was only half the total measurement time. By chopping within the field and combining the images, these limits should be ∼0.4 magnitude fainter. The values quoted are based on measurements with objective L4 and should be ∼0.1 mag fainter in S3 based on their relative efficiencies. Extrapolation to other s/n ratios and integration times can be made assuming s/n $\alpha\ t^{1/2}$ where $t$ is the total integration time.

Table 4 summarizes the 1–2.5 μm limits as defined above achievable using $N_2$ (dark-current-limited) and He (background/read-noise-limited) cooling. The IRAC2 limits have also been included for comparison.

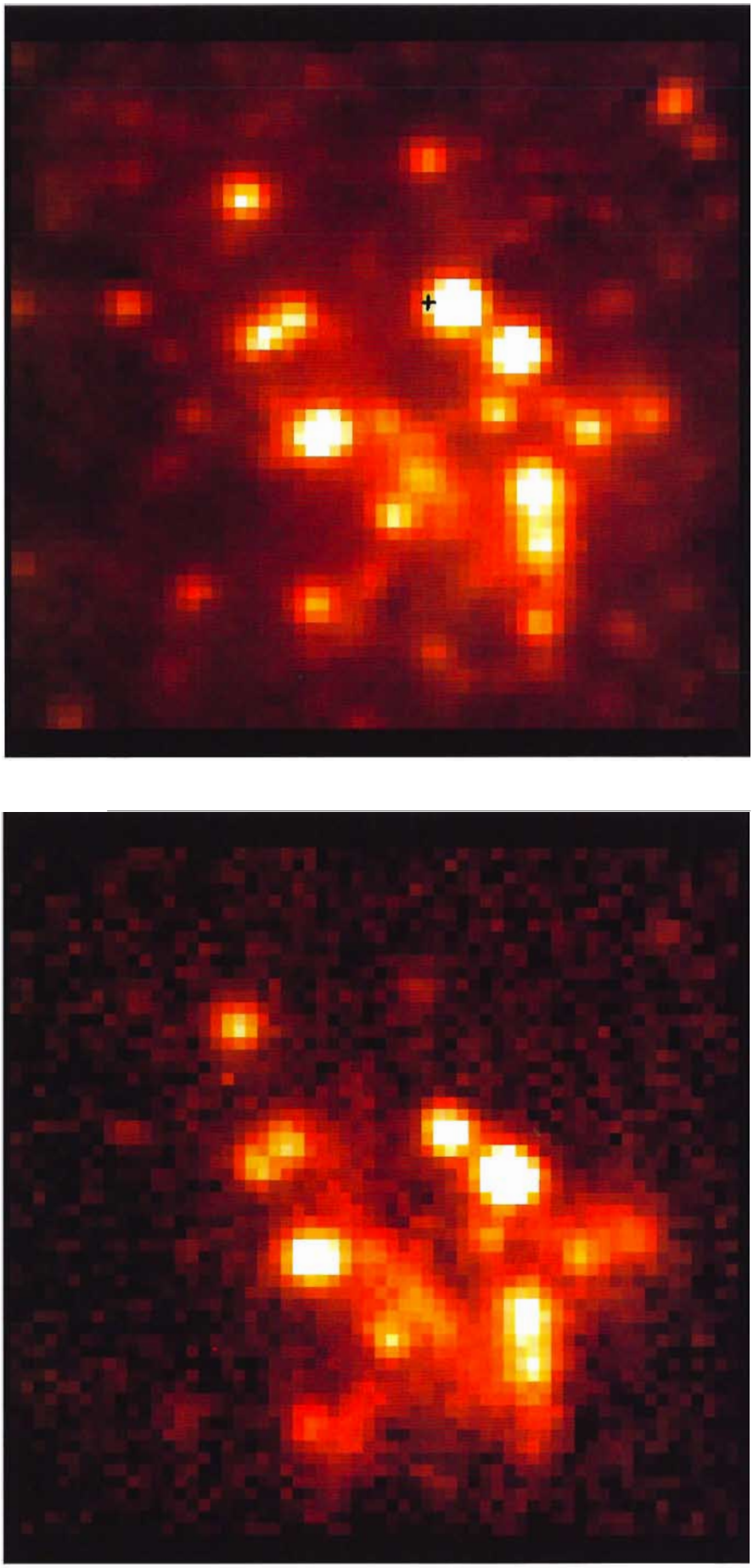

Figure 2: *Images of the Galactic centre in the L′ (3.75 μm) (upper) and MN1(4.7 μm) bands obtained using sky chopping and a total measurement time of 2 minutes. The cross on the L′ image just to the E of the brightest source marks the position of SgrA*. The relatively faint source to the N is IRS7 which is the brightest object in the region at 2 μm.*

TABLE 3. *3–5 μm Detection Limits (mag/sq. arcsec at s/n = 3 in 2 × 60 s)*

| Filter | DIT (s) | NDIT | Cycles | Chopping | Mag/sq. arsec |
|---|---|---|---|---|---|
| L | 0.075 | 2 | 2 × 400 | yes | 12.3 |
| MN1 | 0.075 | 2 | 2 × 400 | yes | 9.5 |
| PAH | 0.075 | 2 | 2 × 400 | yes | 11 |
| PAHREF | 0.075 | 2 | 2 × 400 | yes | 12.5 |
| CVF 3.28 | 3 | 2 × 20 | 1 | no | 11 |
| CVF 4.05 | 1 | 2 × 60 | 1 | no | 10.3 |

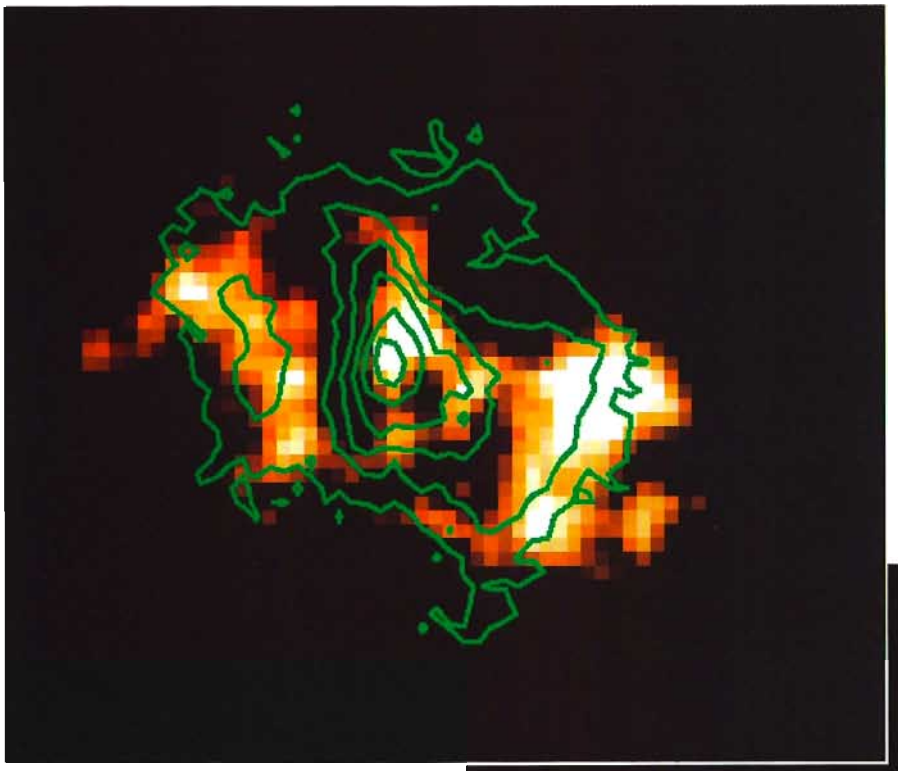

Figure 3: *Image of the Galactic H II region G333.6-0.2 in the 3.28 μm PAH feature with Brα(4.05 μm) hydrogen recombination line contours superimposed. Both features were measured in DC mode using the CVF. The final images in each case were both sky subtracted and continuum subtracted using the mean of images measured on either side of the feature wavelength. Observation times at each CVF position were 60 s and 30 s respectively on both the object and sky positions. Of particular interest is the fact that the PAH feature emission appears brightest at the ionization front to the SW traced by the Brα emission.*

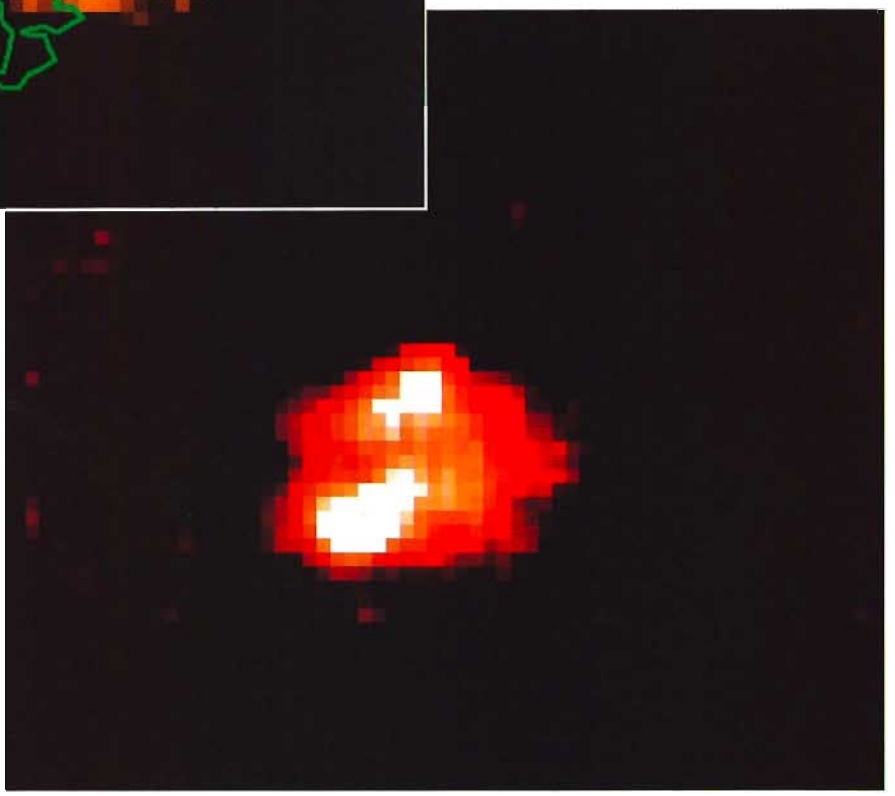

Figure 4: *L′ (3.75 μm)-band image of the starburst ring in the nuclear region of the galaxy NGC 7552 using sky chopping and a total measurement time of 8 minutes. The spatially resolved bright spots correspond to particularly active star forming regions.*

### 3.4 Saturation limits

The brightest objects observable depend on seeing and whether or not defocusing is allowed. As a guide, a point source with integrated magnitudes ~J = 2, H = 2, K = 1.5 measured at the highest frame rate ~50 Hz should just saturate in the brightest pixel assuming it contains 20 % of the light.

### 3.5 Sample images

Figures 2–4 show L′ and MN1-band images of the Galactic centre; CVF images of the 3.28-μm PAH feature and Brα-line emission in G333.6-0.2 and an L′-band image of the starburst galaxy NGC 7552 which illustrate some of the main capabilities of IRAC1 in the thermal infrared. All images are oriented with N at the top and E to the left and have a scale of 0.45"/pixel. Additional specific information is given in the figure captions.


### Acknowledgements

Upgrading IRAC1 with its new detector involved a variety of optical, mechanical, electronic and software modifications as well as assistance during its reinstallation and test. We are particularly grateful for the support given by P. Biereichel, B. Delabre, A. van Dijsseldonk, J.-L. Lizon, G. Huster, M. Meyer and G. Nicolini in Garching and A. Moneti and U. Weilenmann on La Silla.


TABLE 4. *1–2.5 μm Detection Limits (mag/sq. arcsec at s/n = 3 in 2 × 60 s)*

| Filter | mag/sq. arcsec ($N_2$) | mag/sq. arcsec (He) | mag/sq. arcsec |
|---|---|---|---|
| | Lens S3/L4 | Lens S3/L4 | IRAC2 |
| J | 17.3/16.7 | 19.2/18.8 | 20.5 |
| H | 17.2/16.6 | 18.6/18.4 | 19.2 |
| K | 16.7/16.1 | 17.8/17.6 | 18.3 |
| CVF 1.6 | 14.5/14.0 | 16.9/16.3 | |
| CVF 2.166 | 14.2/13.6 | 16.6/16.0 | |